Wind-Induced Vibration and Wind-Driven Rain Performance of a Full-Scale Single-Skin Facade Unit with Vertical Protrusions

Kehinde J. Alawode, S.M.ASCE[1]; Krishna Sai Vutukuru, Ph.D.[2]; Amal Elawady, Ph.D.[3]; Seung Jae Lee, Ph.D.[4]; Arindam Gan Chowdhury, Ph.D.[5]; and Guido Lori, Ph.D.[6]

Abstract: Vertical protruding elements are popularly used for building aesthetics, solar shading, and reduction of energy demand. However, no sufficient design guidelines are available yet for wind loading on curtain walls, especially those with vertical protrusions. In addition, water intrusion tests carried out by curtain wall manufacturers use static or pseudo-dynamic wind loads according to available testing manuals which are not realistic to simulate extreme wind and wind-driven rain conditions. This study investigates the influence of vertical protruding elements on the overall wind actions on a single skin façade using full-scale testing. The results show that vertical protrusions can increase the pressure around the protrusions and the wall (as evidenced by increased pressure coefficients) by as much as 30% and 19%, respectively. Furthermore, the vertical protrusions used in this study increased the overall stiffness of the curtain wall system, which led to an increase in the vibration of the glass units. Wind-driven rainwater intrusion tests on a façade unit without vertical protrusions indicate an increase in water penetration with wind speed at vulnerable joints (i.e., joints with windows) and less than 5 mL at the non-vulnerable joint at all wind speeds tested. **DOI: 10.1061/JAEIED.AEENG-1393**.

Author keywords: Wind-induced vibration; Wind-driven rain; Curtain wall; Vertical protrusions; Water intrusion; Solar shading.

Introduction

Glazed curtain walls are a type of building envelope that primarily serve the purpose of separating and protecting the interior of the building and its contents and/or occupants from the exterior environment. With recent improvements in glass-coating technology, architects have increasingly used glass curtain walls as façades in mid- and high-rise buildings for many reasons, including the enhanced corrosion resistance of the envelope and reduction of building energy consumption, in addition to other incentives, such as great natural lighting and recyclability of glass (Pariafsai 2016). A glass curtain wall system generally comprises glass layers, fasteners or structural sealants, and the support system (which could be frames or point supports alongside cables). Insulation is a major consideration for buildings with glass façades, as insulation affects the overall building energy demand for thermal and visual comforts (Sayed and Fikry 2019). Therefore, with the growing need for energy efficient buildings, the adoption of vertical or horizontal shading devices that are usually protruding from buildings façades is increasing. These help to reduce the amount of sunlight entering the building and also have aesthetic appeal. To further improve the sustainability and energy efficiency of the building, some building owners add photovoltaic panels to these protrusions and parts of the glazed area (Mandalaki et al. 2012).

Many previous studies focused on the cooling and energy-saving performance of various types of shading devices, such as Cho et al. (2014) and Evangelisti et al. (2020). However, little attention has been paid to (1) the effect of these external shading devices on wind pressure distribution (Rofail and Kwok 1999), (2) the associated wind-induced vibration (WIV) of the façade system, and (3) how WIV may relate to the amount of water intrusion from heavy rains that may be associated with extreme wind events. In addition, ASCE 7-16 suggests considering no dynamic effects when the natural frequency is higher than 1 Hz. Although this criterion was developed for the entire building, it proved to be misleading for building components by many previous researchers, such as Strobel and Banks (2014), Moravej et al. (2015), Habte et al. (2015), Cain et al. (2015), Naeiji (2017), Azzi et al. (2020), Estephan et al. (2021), and Vutukuru et al. (2021). Strong winds and wind-driven rain (WDR) are two events that often occur together in nature, especially during hurricane landfalls, impacting building envelopes. Losses due to hurricanes have risen from about $1.3B in 1985 to about $90B in 2017 (NCEI 2019). Damage to properties due to water intrusion exacerbated by WIV through the building envelope is a major cause of these losses (FEMA 2005). Hurricane Andrew in 1992 damaged about 125,000 homes (Fronstin and Holtmann 1994), while Hurricane Katrina in

[1]Ph.D. Candidate, Dept. of Civil and Environmental Engineering, Florida International Univ., Miami, FL 33174. ORCID: https://orcid.org/0000-0003-0281-7789. Email: kalaw003@fiu.edu

[2]Senior Engineer, Thornton Tomasetti, Fort Lauderdale, FL 33301. ORCID: https://orcid.org/0000-0002-5587-5045. Email: kvutukuru@thorntontomasetti.com

[3]Assistant Professor, Dept. of Civil and Environmental Engineering, Florida International Univ., Miami, FL 33174 (corresponding author). ORCID: https://orcid.org/0000-0003-4927-0709. Email: aelawady@fiu.edu

[4]Associate Professor, Dept. of Civil and Environmental Engineering, Florida International Univ., Miami, FL 33174. ORCID: https://orcid.org/0000-0002-2180-3502. Email: sjlee@fiu.edu

[5]Professor, Dept. of Civil and Environmental Engineering, Florida International Univ., Miami, FL 33174. Email: chowdhur@fiu.edu

[6]Group Innovation and Technology, Permasteelisa S.p.A, Vittorio Veneto, Treviso, Italy. Email: g.lori@permasteelisagroup.com

Note. This manuscript was submitted on October 30, 2021; approved on October 31, 2022; published online on January 18, 2023. Discussion period open until June 18, 2023; separate discussions must be submitted for individual papers. This paper is part of the ***Journal of Architectural Engineering***, © ASCE, ISSN 1076-0431.

Table 1. Comparison of previous works on vertical protrusions and this study

Study	Model length scale	Model dimension (full scale)	Major findings
Stathopoulos and Zhu (1990)	1:400	$D = 1$ and 2 m $B = 0$ and 1.4 m $S = 2$ m	For high- and low-rise buildings, vertical protrusions cause high suction at wall edges.
Chand and Bhargava (1997)	1:400	$D = 4$ m $B = 4$, 28 m $S =$ N/A (one protrusion used)	Distance from the edge of the wall determines the effect of vertical protrusions. Protrusions at the extreme edge of the wall increase wall pressures, while those away from the edge reduce wind pressure between the protrusion and the edge.
Yang et al. (2020)	1:300	$D = 2.25$ and 3.75 m $B = 4.5$ and 9 m $S = 4.5$, 12 and 21 m	Depending on the arrangements, vertical protrusions may increase or decrease mean along-wind layer force in high-rise buildings. Continuous vertical protrusions decrease fluctuating across-wind force in high-rise buildings.
Liu et al. (2020)	1:300	1:300	Vertical protrusions modify configuration of shear layer flow and, hence, reduce fluctuating across-wind forces in high-rise buildings.
This study	1:1	$D = 0.28$ m $B = 0.89$ m $S = 1.8$ m	

Note: D = depth of protrusion; B = distance of first protrusion from edge; and S = spacing of protrusions.

2005 affected up to 352,930 homes (FEMA 2006). In addition to the interior losses from water intrusion, the deposition of rainfall on building façades affects hygrothermal performance and durability of the façade, and the heat, air, and moisture (HAM) transfer performance and energy consumption of a building (Baheru et al. 2014; Blocken and Carmeliet 2004).

One of the first systematic 3D experimental studies to investigate the performance of façade systems and the effects of vertical protrusions on wind pressures on walls was carried out by Stathopoulos and Zhu (1990) using both open and urban area terrain exposures. Their results show that the effects of vertical protrusions are more pronounced at the building edges and decrease as from the edges to the center when wind direction is normal to the wall surface. There was a 58% increase in the mean wind pressure coefficient (Cp_{mean}) at the edge of the wall before the vertical protrusion in comparison with a model without vertical protrusions. Also, a change in the terrain exposure showed little to no effect on the Cp_{mean} on the walls with vertical protrusions. This could be due to the use of gradient velocity (i.e., wind velocity at gradient height of atmospheric boundary layer) as the reference in calculating the wind coefficient values. In their studies, Stathopoulos and Zhu (1990) reported that the wind direction of 105° was identified as critical for high suctions in both high- and low-rise buildings with vertical protrusions.

Chand and Bhargava (1997) considered the effects of both vertical and horizontal protrusions on wind pressure coefficients using wind tunnel testing. They concluded that the effect of vertical protrusions on wind pressure distribution on a wall depends on the distance from the protrusion to the edge of the wall. The study found that having protrusions at the wall edge resulted in increasing wind pressure at the corners, while having protrusions at a distance from the wall edge resulted in reducing wind pressure at points between the protrusion and the wall edge. Stathopoulos and Zhu (1990) observed a 58% increase in Cp_{mean}, a 167% increase was observed in Chand and Bhargava (1997) for specific pressure taps relatively at similar positions (top part of model). Note that in this study, suction was observed at the bottom pressure tap between the wall edge and the protrusion, at wind parallel to vertical protrusions, which was similarly observed by Stathopoulos and Zhu (1990).

Recent studies have majorly focused on the effects of these protrusions on the aerodynamic loads (i.e., base moments and across and along wind forces) on tall buildings (Yang et al. 2020). Also, few numerical studies assessed the effect of shading devices on the magnitude of the resulting wind pressure coefficients, such as Zheng et al. (2020), where the 60° to 75° angle of the external shading louvers measured from the horizontal axis provided the most reduction in wind pressure. In addition, a majority of the existing experimental studies on the effects of vertical wall protrusions did not present the pressures on the vertical protrusions, except for Yang et al. (2020). In all these previous studies, neither WDR nor WIV was considered, but rather a wind pressure distribution and/or overall wind force effects on the building were reported. Table 1 provides a detailed comparison regarding the parameters and assumptions considered in each of the mentioned studies and the current study.

In accounting for the coupled effects of simultaneous wind and rain on curtain walls, several standards are used in the glass curtain wall industry to test the watertightness of units. In addition, some field test standards exist to check the effectiveness of already installed units in protecting occupants from water intrusion. The American standards include AAMA 501.1-05 2005 (AAMA 2005); ASTM E1105-15 (ASTM 2009); ASTM E331-00 (ASTM 2016a); and ASTM E547-00 (ASTM 2016b), while the European standards include EN 12155:2000 (CEN 2000); EN 12865 (CEN 2001a); EN 13050:2011 (CEN 2011b); and EN 13051:2001 (CEN 2001b). Uniform static air pressure difference is the method to apply the wind load per ASTM E331; Procedure A of ASTM E1105-15 (ASTM 2009); EN 12865 (CEN 2001a); and EN 13051 (CEN 2001b). The test procedure involves a static pressure difference maintained for 5–15 min while the water spray is applied. The static pressure difference applied is a percentage (usually around 15%–40%) of the design pressure of the cladding because peak rainfall does not always correspond to the highest wind speeds except during extreme wind events. As the standards are developed for general use, the peculiarity of hurricane-prone zones is not included. The water sprays, together with the static air pressure while being used to represent WDR effects on the surface of the specimen, are not designed to match any previous rain event. Table 2 gives a summary of the requirements for each of the codes for water intrusion testing on curtain walls.

In hurricane-prone areas designated as a high-velocity hurricane zone (HVHZ), such as Miami-Dade County in USA, the Florida Building Code (FBC) Test Application Standards (TAS) is used. TAS 202 (ICC 2017a) and TAS 203 (ICC 2017b) resemble ASTM E331-00, with no water intrusion expected at 15% of design pressure and constant water spray while the test specimen might be subjected to a missile resistance test (either two 2 g balls hurled at 40 m/s or 4.1 kg of wood hurled at 15.2 m/s on the glass surface) before the water intrusion test, making the test more onerous.

Despite the adherence to these standards, water intrusion in high-rise buildings with glass curtain walls during rain and wind events is frequent. This has led to questions regarding the validity and effectiveness of current curtain wall water intrusion testing procedures in the standards in replicating realistic wind and rain conditions.

Table 2. Details of requirements of various curtain wall water intrusion testing codes

Standard test	Type of load	Specified load	Specified number of cycles	Objective	Water spray rate
ASTM E331	Static[a]	137 Pa	Unspecified	Lab test	3.4 L/m^2 · min
ASTM E1105-05(A)	Static	Unspecified	Unspecified	Field test	3.4 L/m^2 · min
ASTM E1105-05(B)	Cyclic[b] static	Unspecified	Minimum of 3	Field test	3.4 L/m^2 · min
ASTM E547-00	Cyclic static	137 Pa	Unspecified	Lab test	3.4 L/m^2 · min
EN 12155	Static	Depends on rating pressure	Unspecified	Lab test	2 L/m^2 · min
EN 13050	Dynamic[c]	0.375 of Design Pressure	Unspecified	Lab test	2 L/m^2 · min
EN 13051	Static	No loads, Annex B suggests the use of EN 12155 loadings if air pressure is required	Unspecified	Field test	5 L/min per meter length of spray bar
EN 12865	Pulsating load	Steps of 150 Pa	As much as needed	Lab test (Limit of watertightness)	Run-off - 1.2 L/(m · min) Driving rain - 1.5L/(m^2 · min)
AAMA 501.1-05	Dynamic	300.0, 380.0, 480.0, 580.0 and 720.0 Pa.	One 15 min cycle at a time	Lab test/Field test	3.4 L/m^2 · min
TAS (202)	Uniform static	15% of wind design pressure based on 75 mph wind velocity	15 min	Lab test	3.4 L/m^2 · min

[a]A specific static pressure difference is maintained between the wall of a test chamber and the glass surface.
[b]A specific static pressure difference is maintained between the wall of a test chamber and the glass surface, then brought down to zero in 1 min, and the process is repeated.
[c]A specified airflow from fans and continuous regular pulses of static pressure difference is maintained between the wall of a test chamber and the glass surface.

Some researchers (Baskaran and Brown 1995; Van Den Bossche et al. 2013a; Pérez-Bella et al. 2013) stated that the reason for the occurrence of water intrusion in curtain walls is that standardized tests do not accurately simulate the wind-driven rain (meteorological conditions) that curtain wall systems are exposed to in the field. In addition, field tests using airplane engine fans might not simulate the frequency range of turbulent winds and water intrusion tests, but only subject the curtain walls to a small percentage of the peak pressures expected in the lifetime of the structure.

Factors affecting WDR on a building façade include the upstream wind conditions, local flow pattern around the building, rainfall intensity, and raindrop distribution (Choi 1993). Measurement of WDR has evolved over the years. Many researchers have used different names to express the quantity of WDR; these include specific catch ratio, catch ratio, local effect factor, local intensity factor, driving-rain ratio, or rain admittance function. Blocken and Carmeliet (2004) provided a detailed review of methods of WDR investigation. The measurement of WDR can be grouped into empirical, semi-empirical, and numerical methods (Blocken and Carmeliet 2004; Derome et al. 2017; Orr and Viles 2018). Pressure difference is the primary parameter determining water intrusion in the curtain walls, especially in openings smaller than 1 mm in size, but WDR becomes an equally dominant parameter in façades with drains or openings larger than 5 mm in size (openings smaller than 1 mm are considered normal, while openings larger than 5 mm are considered as defects) (Cornick and Lacasse 2005; Van Den Bossche et al. 2013b). Realistic reproduction of coupled wind and rain conditions in pre-installation testing is lacking in the current pressure and watertightness testing standards worldwide. Pérez-Bella et al. (2013) and Van Den Bossche et al. (2013b) provide a methodology to measure watertightness in an event of simultaneous rain and wind by suggesting the use of a Pareto analysis method to select the appropriate combination of wind speeds and rainfall intensity using metrological data for each area, instead of the continuous water flow prescribed by current water intrusion testing standards. Kubilay et al. (2015) reported field measurements and computational fluid dynamics (CFD) simulations of WDR at the Swiss Federal Laboratories for Materials Science and Technology. The study focused on assessing the WDR intensity on two parallel wide buildings at different positions on the building's envelopes. The study showed that the presence of surrounding buildings highly affects the intensity of WDR on a building. Similarly, wind pressures on building surfaces are also affected by the presence of surrounding buildings (Taniike 1992). The study by Choi (2008) indicates that the increase in the dynamic pressure on building façades due to the occurrence of the combined actions of wind and rain is only 2.2%. A similar conclusion was reached by Liu et al. (2019). However, neither study considered water intrusion.

WIV on glazed curtain walls has been investigated through experimental and numerical studies as well as field measurements. Vibration in curtain walls is usually ignored. Because the natural frequency of these systems is typically higher than 1 Hz, the structural design codes of practice assume that glazed curtain walls systems are not susceptible to wind excitations (ASCE 7-16, ASCE 2016). Zhengnong et al. (2011) recorded the field measurements of vibration, strains, and stresses of glass façades due to wind and heavy rain during three typhoon landings in Xiamen, China. Their field data collection was on a 150 m-high building with a façade having two layers of 8-mm tempered glass sized 1,400 × 1,700mm with 12-mm air space. Their results indicated that the mean principal strain at the center of the glass panel showed a similar trend to the changes in wind pressure time history, with a reduced strain at the sides of the panel due to the constraints of the frame's support (i.e., transoms and mullions). Also, a linear relationship was observed between the stresses in the glass and the wind pressure. One of the monitored glass panels had both positive and negative stresses, which indicates that the panel was under alternating actions of pressure and suction. The wind pressures noted during the typhoons were lower than the designed pressure capacity of the glass façade.

Yu et al. (2017) conducted an analytical study to measure wind-induced response of an L-shaped glass curtain wall that was the corner segment of a building in Fuzhou, China. The glass curtain wall is supported by prestressed cables, designed for a wind speed of 33.5 m/s. The glass panels are connected using sealants and fasteners. The authors performed a time domain fluid-structure interaction analysis using ADINA finite-element software.

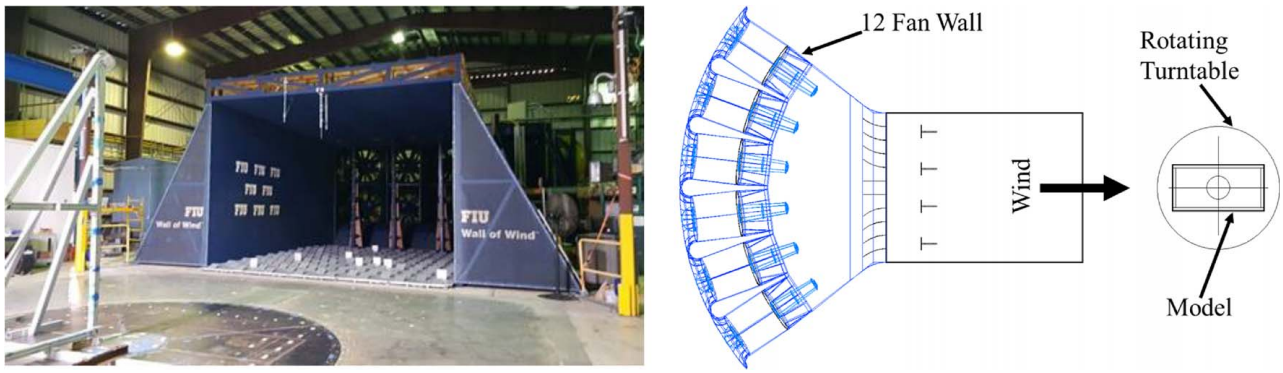

Fig. 1. WOW EF: (a) test section; and (b) floor plan.

A fluctuating wind load only in the along-wind direction is applied using a generated wind speed time-history with a target Kaimal spectrum. A wind vibration coefficient based on Davenport's gust response theory was used as a measure of wind dynamic amplification. The first few modes of this cable-supported façade ranged from 1.5 to 2.5 Hz. The wind displacement vibration coefficient (defined as the ratio of maximum to mean displacement) was ~2.0 for wind directions ranging from 0° to 45°. They concluded that wind direction has little effect on acceleration response. Nakagami (2003) simulated wind loads on two different façades supported either at certain points or along the edges. The analysis was conducted using an ANSYS finite-element package for a peak wind velocity of 30 m/s. The results indicate that the linear-edge support system had 10% less deformation compared with the point supported system. The author evidenced that the natural frequency of the façade depends largely on its surface area and support conditions, while noting that double-glazed units have a higher possibility of vibration at resonant frequency.

This research project was motivated by the lack of guidance in major wind loading standards (i.e., Eurocode and ASCE 7) regarding the effect of vertical protrusions on the response and loading of curtain walls and the watertightness performance of the system during extreme wind events. Previous studies have considered wind pressures, WDR, and WIV separately, or carried out WDR tests using methods that do not fully incorporate the turbulence of the atmospheric boundary layer (ABL). There is a knowledge gap in the correlation of WDR and WIV for glazed curtain wall systems that must be addressed, especially as the response of glazing is dependent on the stiffness of its supports. Also, with the increasing use of vertical protrusions, it is necessary to know their effect on the wind loads on the curtain wall. The study is expected to bridge this gap. An experimental investigation using ABL winds was conducted to understand the influence of WIV and WDR on water intrusion in a glazed façade (a unitized aluminum-framed unit) supplied with vertical shading devices. The experimental program was designed to investigate the influence of vertical shading devices on wind pressure and glass accelerations in single-skin façade units. The configurations tested may represent the first floors near the ground, where there is usually a higher wind turbulence. The second section of this paper details the experimental setup, materials, and methodology used. The third section discusses the experimental results. Conclusion and a summary of major findings are provided in the final section.

Fig. 2. Supporting steel frame.

Experimental Setup and Data Analysis Method

Experimental Facility and Model Configuration

The Wall of Wind (WOW) Experimental Facility (EF), Florida International University, is an open jet, large wind tunnel with a 2 × 6 array of fans in an arc-focal arrangement. The facility is capable of testing large-scale models at up to Category 5 hurricane wind speeds of ~70 m/s (Chowdhury et al. 2017, 2018) and a unique advantage of high Reynolds number simulations of wind and WDR effects. Fig. 1 shows the 4.9 m diameter turntable and flow management box and the schematics of the WOW EF, respectively.

Permasteelisa provided the curtain wall, which comprises three façade units with overall dimensions of 3.65 m width by 3.18 m in height. These are mounted on a rectangular supporting steel structure of 3.65 m (width) × 3.18 m (height) × 1.83 m (depth), shown in Fig. 2, and a flat roof with 0.41 m overhangs. Two test configurations were tested in this study: the configuration "without vertical protrusions" (Model A) that served as a reference model, and the configuration "with vertical protrusions" (Model B). Figs. 3 and 4 show photos of the Model A and Model B configurations mounted on the WOW EF turntable, respectively. Model B has two protruding V-shaped vertical aluminum protrusions, as shown in Fig. 5(a). Dimensions of the curtain wall in both models are shown in Fig. 5(b). The unit is double-glazed, composed of inner and outer glass layers that are separated by a thermal spacer, as shown in Fig. 5(c). Fig. 6 shows the glass zones and framing profile locations

(a) (b)

Fig. 3. Model A without vertical protrusions: (a) actual curtain wall side; and (b) polycarbonate on wooden frame side.

on the curtain wall unit. Table 3 gives the thicknesses of the glass layers. Some of those glazing have a laminated inner glass consisting of two glass layers and a polyvinyl butyral (PVB) interlayer. Fig. 7 shows the profile cross sections. On both configurations, the other side of the wall has three panels of clear polycarbonate plates. This polycarbonate wall allows for the placement of pressure taps because it is impractical to drill the actual glass curtain wall. Wooden vertical protrusions representing the actual aluminum vertical protrusion (i.e., fins) were added to the polycarbonate side of Model B. The two sides on the 1.83 m length of the test model were closed with wood panels. All the walls were fixed to a steel frame, bolted to the turntable in the testing chamber. The steel frame provided high rigidity, as needed for running high-wind velocity tests.

The model is nominally sealed as evidenced by the 0.0365 root mean square (rms) of internal pressure coefficient. Guha et al. (2011) stated that the rms of internal pressure coefficient of nominally sealed buildings is around 0.05. Also, mean internal pressure was about 2.2 kPa less than the mean external pressure of a centrally located pressure tap. The model blockage to the wind tunnel, based on flow management box area, is 45%. This is higher than the 5% recommended for closed- or open-circuit wind tunnels, whereas the WOW is an open jet wind tunnel.

Testing Protocol and Instrumentation

In this study, an open terrain ABL wind profile was simulated. Wind speed and turbulence characteristic measurements at the center of the turntable were measured with Cobra probes instruments. The mean wind speed at the reference height (roof height) (3.2 m) of the test model is 21.97 m/s. Fig. 8 shows the power spectrum density (PSD) at the reference height (z_{ref}), mean wind speed, and turbulence intensity profiles, and fluctuating turbulence generated at WOW EF, compared with those produced using ESDU item 85020 (ESDU 2001) with a roughness length (z_0) of 0.08 m (this falls within the range of open-terrain exposure). As expected for large-scale testing, PSD shows that a portion of the low-frequency fluctuations is missing in the wind simulation, the effect of which is incorporated using post-test analytical procedure using the partial turbulence simulation (PTS) method. The PTS method was developed and validated at the WOW EF (Mooneghi et al. 2016; Moravej 2018) to incorporate the effect of low-frequency turbulence that is not simulated in a large- and full-scale testing. Table 4 details the testing protocol and duration, whereby the pressure test indicates pressure measurement on the polycarbonate wall and kinetic test represents acceleration and strain measurements on the actual curtain wall.

(a) (b)

Fig. 4. Model B with vertical protrusions: (a) actual curtain wall side; and (b) polycarbonate on wooden frame side.

Pressures on (1) the polycarbonate wall, (2) the wooden fins, and (3) the inside of the model were measured using a total of 112 pressure taps (110 taps on the polycarbonate wall and two taps inside the test building) for Model A. An additional 16 taps were instrumented on the vertical protrusions for Model B, for a total of 128 taps. The pressure taps had a denser resolution at the wall edges to ensure that the variation of pressure at those sharp edges were captured appropriately. Fig. 9 shows the pressure tap locations on the polycarbonate wall. Each tube measuring 2.7 m was connected to the ZOC Scanivalve pressure scanner module. Wind pressure data were acquired at a 512 Hz sampling frequency for a duration of 1 min. A tubing transfer function (Irwin et al. 1979) was used in the analysis, given the 2.7 m length of tubes adopted due to the full-scale model size. Wind direction varied from 0° (windward direction on polycarbonate wall) to 345° at 15° increments by rotating the turntable as shown in Fig. 10.

Accelerometers were attached to the glass of the curtain walls while strain gauges were attached to the back of the mullions. Fig. 11(a) shows a schematic of the layout of the accelerometers and strain gauges, and Fig. 11(b) shows Accelerometer A3.

WDR Test for Model A

A full-scale (1:1) raindrop size with matching characteristics (i.e., rain rate and rain drop size) was developed in the WOW EF.

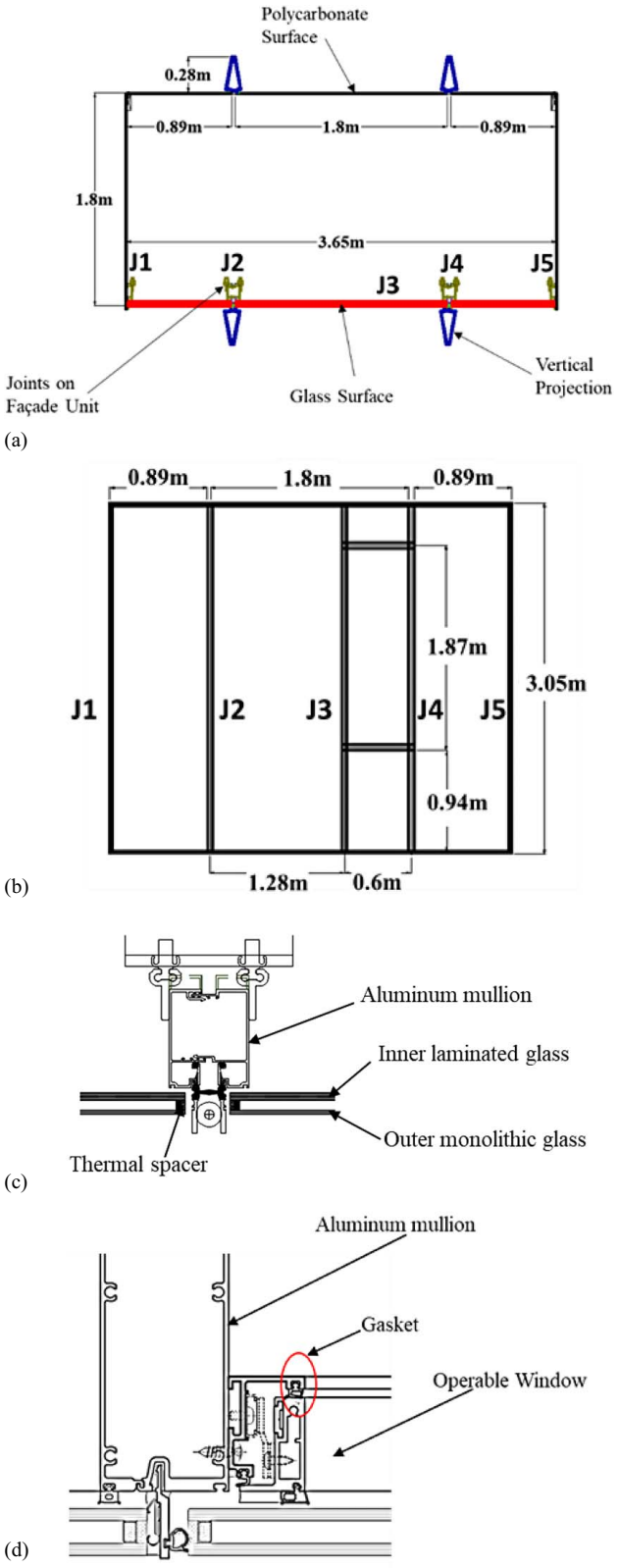

Fig. 5. Schematic overview of test model: (a) plan view of test Model B; (b) elevation view of Model A; (c) section along Joint 2 (J2); and (d) section along Joint 3 (J3).

This was an advancement over the existing 1:4 rain drop-size distribution developed by Baheru et al. (2014). A normalized gamma distribution curve was utilized to match the raindrop size with concentration (Tokay et al. 2013) to obtain the right raindrop

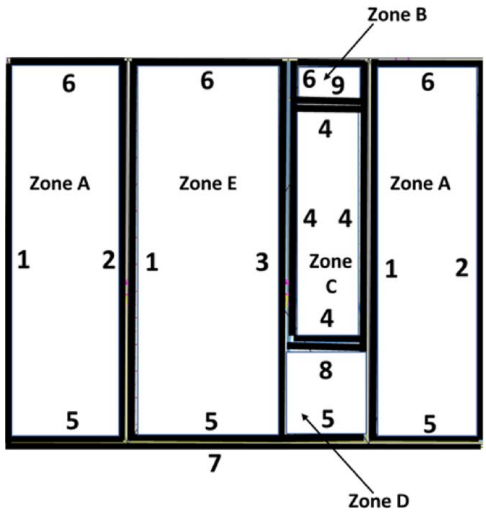

Fig. 6. Glazing zones and framing profiles' location.

distribution with a rain rate of 223 mm/h, as suggested by AAMA 501.1. Typically, water intrusion tests for façade pass/fail assessment are performed using an airplane engine under static wind conditions. However, to ensure accuracy and to replicate realistic hurricane rain characteristics, a gamma-fitted model developed by Tokay et al. (2013) which uses three real hurricanes of Alex, Charley, and Gaston was utilized as a base model to match rain characteristics. To obtain the correct rain size distribution, 3D printed nozzles were installed in front of the WOW fans. The WDR tests were carried out on Model A only at 22.35, 31.30, and 40.23 m/s wind speeds, as detailed in Table 4. The shorter testing duration at 40.23 m/s was to compensate for higher wind speeds. Other researchers (i.e., Vutukuru et al. 2021) have used a similar approach. The 3D printed nozzle design for these tests is shown in Fig. 12(a) and the best fit for gamma curve for the selected configuration is shown in Fig. 12(b). There was a good match within the rain drop sizes of 1–2 mm, which was the mean rain drop diameters from the investigations of Tokay et al. (2008).

Pig water-absorbing mat (catalog # WTR008) materials were taped strategically at Joints 2, 3, and 4, along the height of the curtain wall unit, as well as on the windowsill. The absorbent materials were weighed before and after each WDR water intrusion test. The difference in weight is the water absorbed by each material. An electronic weighing balance with a precision of 0.001 g was used in this study.

Data Analysis

The pressure coefficients, both mean and peak values, are defined by

$$Cp_{\text{mean}} = \frac{P_{\text{mean}}}{\frac{1}{2}\rho U_{\text{mean}}^2} \tag{1}$$

Table 3. Glazing properties

Glazing zone	Outer glass thickness (mm)	Inner glass thickness[a] (mm)	Gap thickness (mm)
A	6	5 + 0.76 + 5	12
B	6	6	16
C	6	5 + 0.76 + 5	12
D	6	5 + 0.76 + 5	12
E	10	6	12

[a]+ = Glass + PVB layer + Glass.

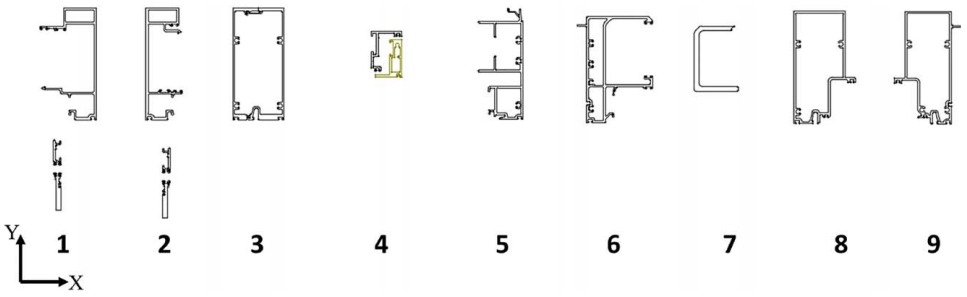

Fig. 7. Framing profile cross sections.

$$Cp_{\text{peak}} = \frac{P_{\text{peak}}}{\frac{1}{2}\rho U_{3s}^2} \tag{2}$$

where U_{mean} and U_{3s} = mean and peak 3s wind speeds at the roof height of the model, respectively; ρ = air density; and P_{mean} and P_{peak} = differential mean and peak pressures, respectively. The peak Cp values were estimated and corrected analytically using the PTS method:

$$Cp_{\text{max,envelope}} = \max_{0^\circ \le \theta \le 180^\circ} \{Cp_{\text{peak}}(k, \theta)\} \tag{3}$$

$$Cp_{\text{min,envelope}} = \min_{0^\circ \le \theta \le 180^\circ} \{Cp_{\text{peak}}(k, \theta)\} \tag{4}$$

where $Cp_{\text{max,envelope}}$ = maximum Cp_{peak} from all wind directions; and $Cp_{\text{min,envelope}}$ = minimum Cp_{peak} from all wind directions.

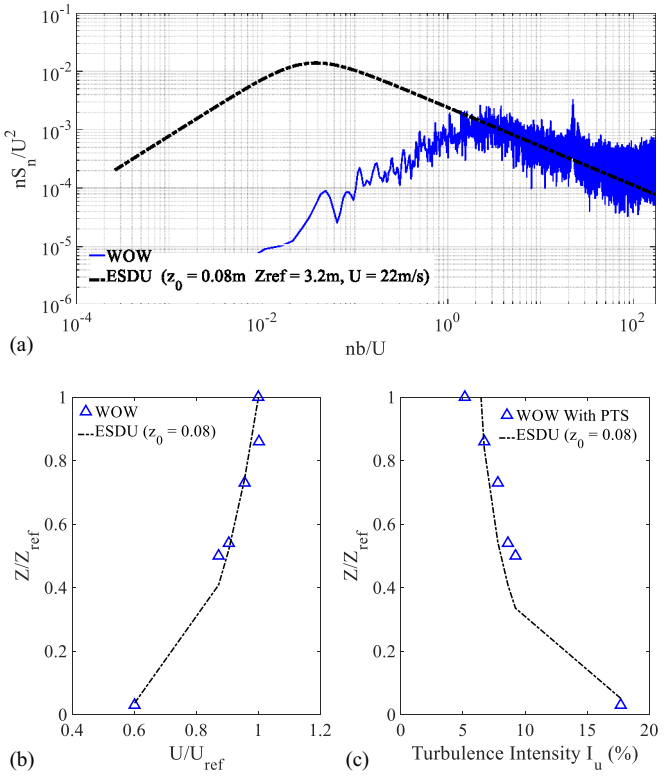

Fig. 8. Comparison between WOW and ESDU: (a) power spectral density function; (b) mean wind speed profile; and (c) turbulence intensity profile.

Results and Discussion

Pressure Distribution

The distribution of the peak pressure coefficients (Cp_{peak}) on the polycarbonate walls of Model A and Model B are compared. Fig. 13 shows the contour plots of Cp_{peak} values at varying wind directions for Model A and Model B.

At 0° (wind normal to curtain wall surface), Cp_{peak} are 12.5% higher in the central panel of Model A compared with those on Model B, as shown in Fig. 13(a). This is contrary to the observation by Stathopoulos and Zhu (1990) and Yang et al. (2020), who showed an increased Cp_{peak} at the central panel for the case with vertical protrusions of 2 and 3.75 m depth, respectively, in full scale. This may be due to the difference in depths of the protrusions in these studies compared with the 0.28 m depth in this study. In addition, this study shows that the vertical protrusions reduce the Cp_{peak} on edge units in Model B, where Cp_{peak} is 10% less when compared with Model A, in agreement with the study by Chand and Bhargava (1997).

At the 15° wind direction, similar Cp_{peak} values and pattern are observed at the left panels and middle panels for Models A and B, while the right panel of Model B indicates lower pressures immediately after the protrusion, as shown in Fig. 13(b). This is due to the blockage effect (i.e., obstacle to wind flow) of the vertical protrusion. Reduction in wall-edge Cp_{peak} values are observed at 0° and 15° due to the vertical protrusion; this was similarly observed by Maruta et al. (1998). From 30° to 60° [shown in Figs. 13(c–e)] the blockage effect of the vertical protrusions increases. At the 30° wind direction, there is a reduced positive pressure at the right edge panel in Model B which is not observable in Model A. Also, Cp_{peak} are higher on the left and middle units of Model B in comparison with Model A. At 45°, compared with Model A, there is an abrupt drop in Cp_{peak} values behind the vertical protrusion on the right side in Model B. A reduction in pressure on the left panel of

Table 4. Testing protocol per configuration

Test type	Wind speed (m/s)	Wind direction (degree)	Test duration (mins.)
Pressure	22.35	0, 15, 30, 45, 60, 75, 90, 105, 120, 135, 150, 165, 180	1
Kinetic	22.35	0, 45, 90, 135, 180, 225, 270, 315	10
Kinetic	31.30	0, 45, 90, 135, 180, 225, 270, 315	5
Kinetic	40.23	0, 45, 90, 135, 180, 225, 270, 315	5
WDR	22.35	0, 15, 345	15
WDR	31.30	0, 15, 345	15
WDR	40.23	0, 15, 345	10

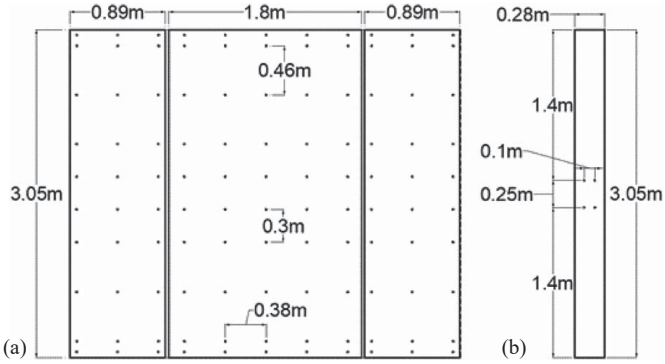

Fig. 9. Tap layout on (a) polycarbonate wall; and (b) wooden vertical protrusion.

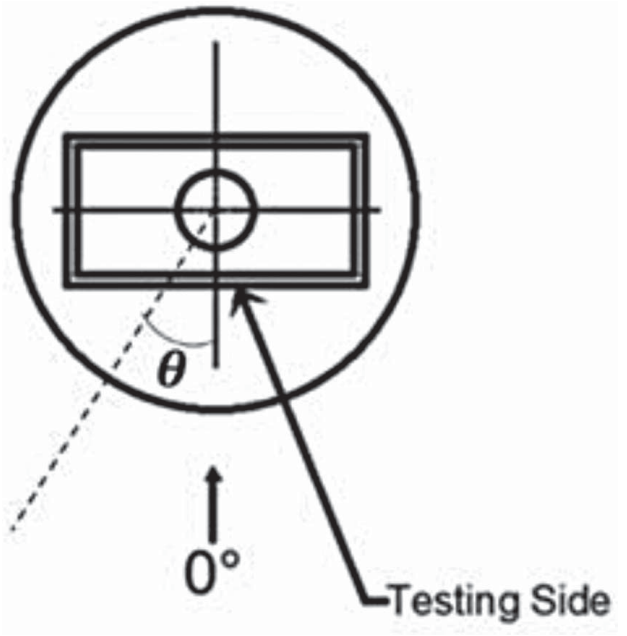

Fig. 10. Wind direction.

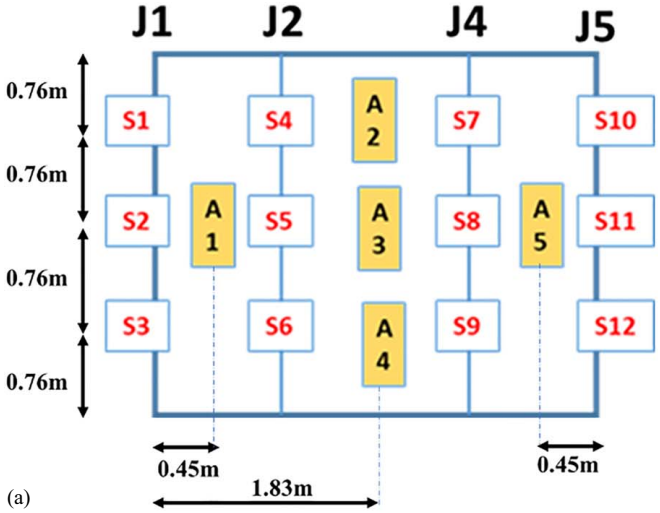

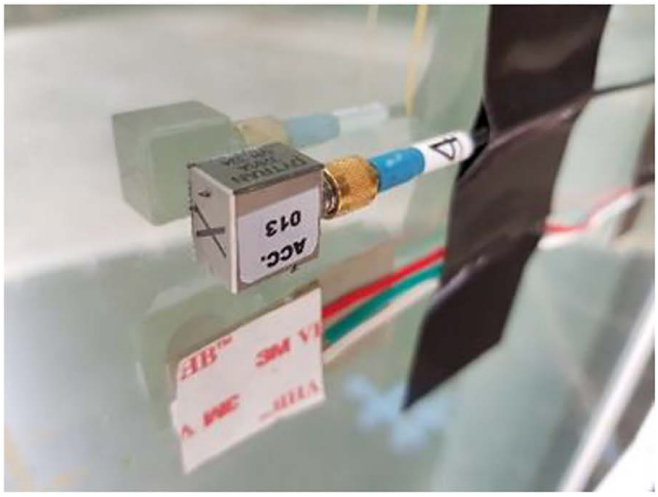

(b)

Fig. 11. Accelerometer: (a) schematic of strain gauge and accelerometer layout; and (b) Accelerometer A3.

Model B is observed in comparison with the 30° data. At the 60° wind direction, there is a full-suction region observed on the middle and right panels of Model B, opposite to the observation on Model A.

The right edge of the walls of Models A and B become separation zones since 75°, with higher suction Cp_{peak} observed at the left unit of Model A in comparison with Model B at both 75° and 90° [shown in Figs. 13(f and g), respectively]. However, at 75° the middle and right units of Model B have higher suction Cp_{peak} in comparison with Model A as vertical protrusions serve as separation points for the incident wind. Contrarily, at 90°, suction across the wall of Model A is higher than those at Model B, which could be due to the formation of recirculation vortices behind the left vertical protrusion that reduces the suction. This observation at 90° is contrary to the observation of Stathopoulos and Zhu (1990), where suction increased in the presence of vertical protrusions for 90° direction. The depth of the vertical protrusions, proximity of the protrusions to the wall edges, and the number of vertical protrusions is different in both studies. These deviations could be the cause of the observed difference, as Stathopoulos and Zhu (1990) opined that the distance of the first protrusion from the edge of the wall plays a significant role in the measured *Cp* values.

The contour plot of the maximum and minimum *Cp* from all wind directions ($Cp_{max,envelope}$ and $Cp_{min,envelope}$) on the walls of Model A and Model B are shown in Fig. 14. The $Cp_{max,envelope}$ at the vicinity of the vertical protrusion in the top part of the wall of Model B are higher than other points on the wall. Similarly, Yuan et al. (2018) observed higher Cp_{max} values at the top parts of the walls. About 30% higher concentration of $Cp_{max,envelope}$ is shown in the vicinity of the vertical protrusions on Model B when compared with Model A, indicating the need for careful installation for the joints supporting such protruding elements. $Cp_{min,envelope}$ values are also lower on Model B in comparison with Model A across the wall, indicating higher suction on the wall.

As shown in Fig. 9(b), the pressure taps on the vertical protrusions are only around the midheight. Pressure measurements on the vertical protrusion show that the pressure coefficients on the protrusions can be higher than the pressure coefficients on the walls. Fig. 15 shows the envelope of the maximum and minimum *Cp* from all wind angles tested on a representative (left) vertical protrusion. The high *Cp* values on the vertical protrusion agree with the expectation of high wind loads on edge protrusions by Stathopoulos and Zhu (1990).

The root mean square (rms) of the *Cp* (Cp_{rms}) along the midheight of the wall is shown in Fig. 16 for 0°, 15°, 30°, 45°, 60°,

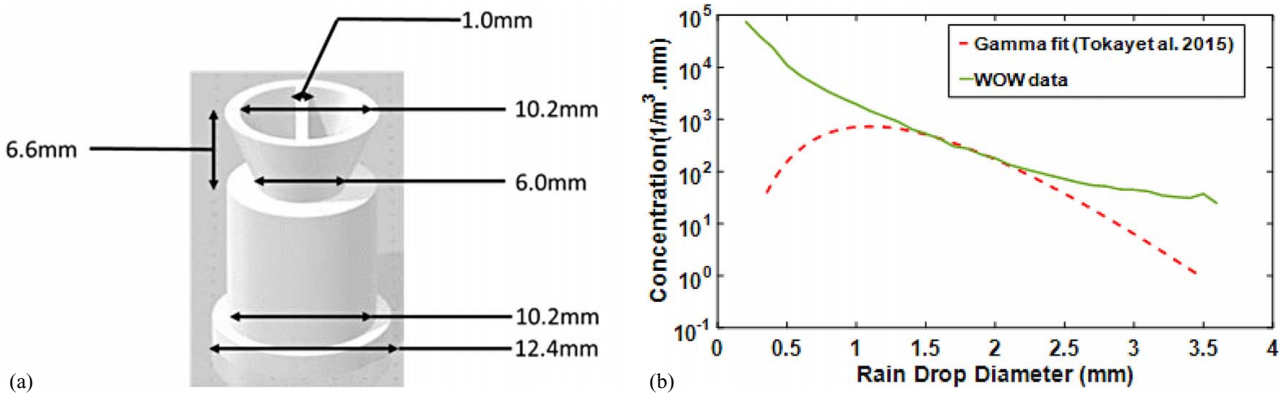

Fig. 12. Nozzle and curve: (a) 3D printed nozzle; and (b) result fitting gamma curve.

75°, and 90° wind directions. The plots indicate that at oblique angles the Cp_{rms} values of Model A gradually reduce from left to right while Model B always shows a sharp reduction in Cp_{rms} values immediately behind the vertical protrusion. Also, the Cp_{rms} values are generally lower in Model B than Model A except at 15° and 30° where there is a higher Cp_{rms} value in Model B when compared with Model A. As higher Cp_{rms} is an indication of higher wind fluctuation, the vertical protrusions may reduce the fluctuations for

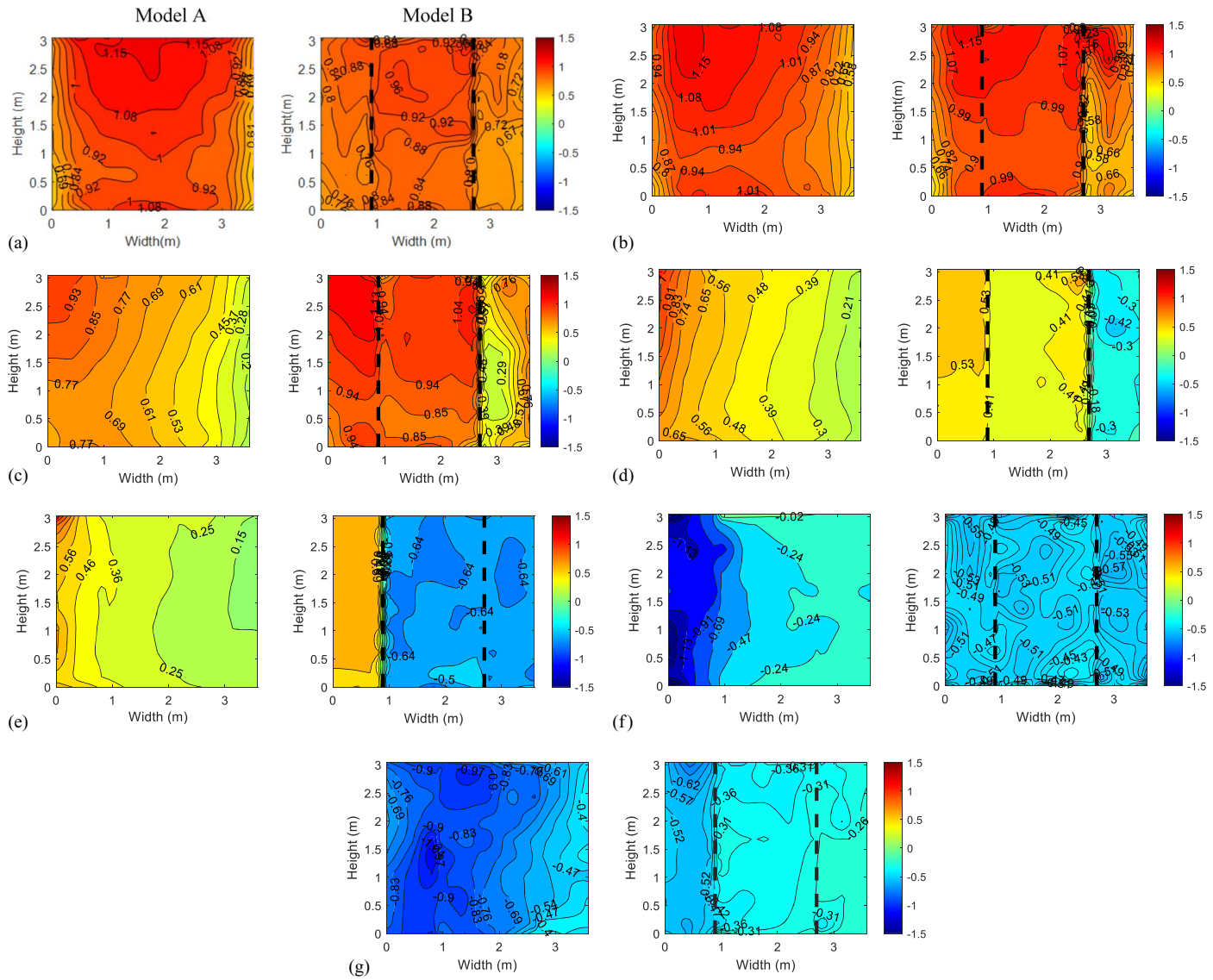

Fig. 13. Cp_{peak} contour plots for Model A and Model B at varying wind directions: (a) 0°; (b) 15°; (c) 30°; (d) 45°; (e) 60°; (f) 75°; and (g) 90° (Model A – left, Model B; dashed lines indicate position of vertical protrusions).

J. Archit. Eng., 2023, 29(2): 04023003

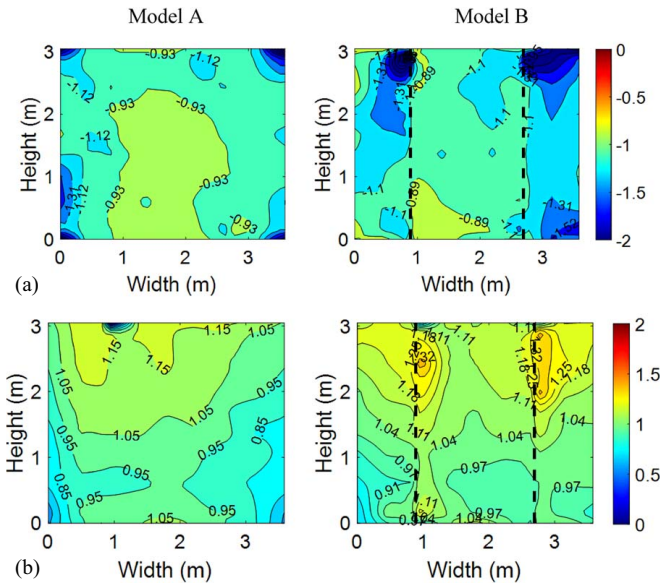

Fig. 14. Envelope of Max *Cp* and Min *Cp* on Model A and Model B: (a) *Cp* Max envelope; and (b) *Cp* Min envelope (Model A – left, Model B; dashed lines indicate position of vertical protrusions).

most wind directions. This is in line with the conclusions by Maruta et al. (1998).

Pressure Coefficient Comparison with Wind Load Provisions

The ASCE 7-16 (ASCE 2016) gives recommendations for design loads on buildings and other structures, including wind loads. The Eurocode (EN 1991-1-4:2005 + A1:2010, CEN 2011a) is the latest European guidance on wind loading for structures.

A comparison between the peak *Cp* values obtained from this study and the wind load recommendations of ASCE 7-16 and EN 1991-1-4:2005 + A1:2010 (CEN 2011a) is presented in Table 5. The ASCE 7-16 recommendations for wind load on components and claddings are in Chapter 30. It should be noted that ASCE

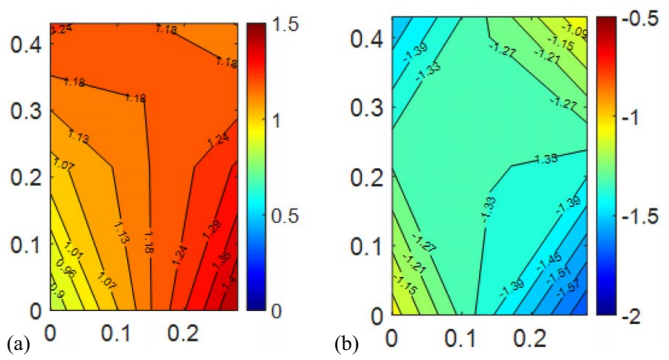

Fig. 15. Envelope pressure coefficient at midheight of the vertical protrusion: (a) Max *Cp*; and (b) Min *Cp*.

7-16 (i) includes the gust effect factors (i.e., G) in the wind pressure coefficients and (ii) recommends that *GCp* values obtained from the equations are reduced by 10% when the roof angle is less than 10°. However, the values presented in Table 5 are not reduced.

The Eurocode specifies Cp_e (external pressure coefficient) values based on the surface area like the ASCE 7-16. Also, the *Cp* values in the Eurocode for a wall are a function of the height-to-depth ratio (h/d). The WOW model has an h/d ratio of 1.75. The Cp_e values in the Eurocode are without the gust factor (G) and are majorly specified with a 10-min average wind speed. St. Pierre et al. (2005) gives a conversion formula simplified as

$$(GC_{pf})_{\text{eq}} = \frac{\left(\frac{V_{10\,\text{m}}}{V_{3s}}\right)^2 (C_e)_{\text{EU}} Cp_e}{K_{zt}K_hK_d} = F_{\text{ENV}} \cdot Cp_e \tag{5}$$

where $V_{10\,\text{m}}$ = 10-min averaged wind speed; V_{3s} = 3-s averaged wind speed; and the ratio of the wind speeds is obtained with Durst curve (Durst 1960). The square of the ratio is 0.48. $(C_e)_{\text{EU}}$ = exposure factor in the Eurocode Section 4.5, given as 1.7 for open terrain and model roof height. K_{zt} is the topographic factor ($K_{zt} = 1.0$), K_h = wind directionality factor ($K_h = 0.85$); and K_d = velocity pressure exposure factor evaluated at mean roof height ($K_d = 1$), all from the ASCE 7-16 section 26, for the case

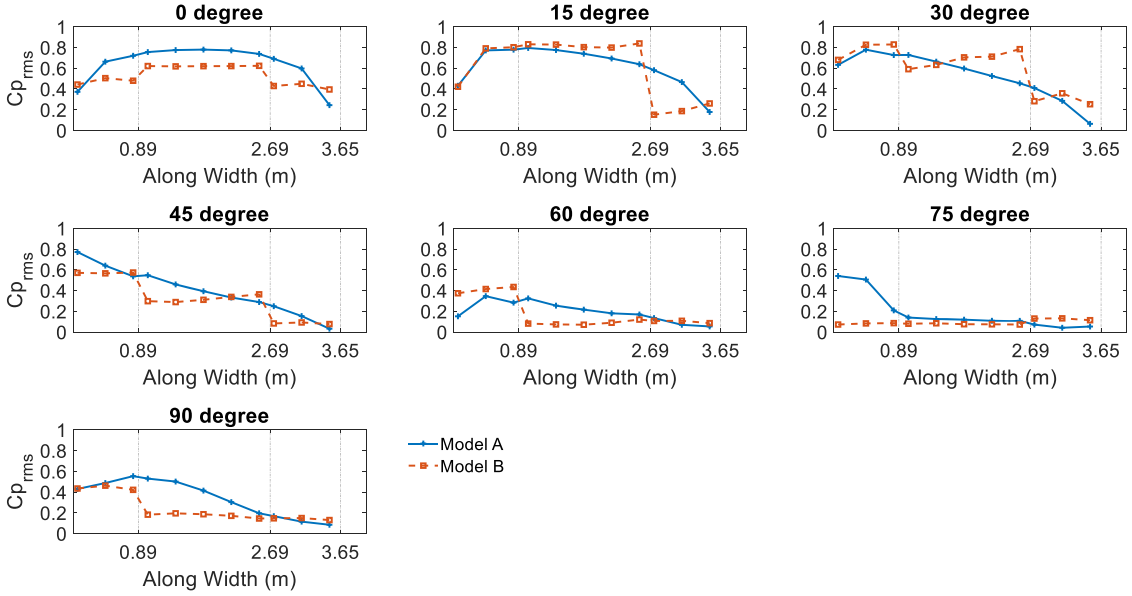

Fig. 16. Rms of pressure along midheight of model.

Table 5. Comparison of external pressure coefficients (GCp) with code provisions

Zone	Pressure sign/direction	ASCE 7-16	EN 1991-1-4	Model A	Model B	% Difference between Model A and Model B
4	(Positive)	0.8637	0.9749	0.9651	1.0724	7.24
	(Negative)	−0.9637	−1.4327	−1.0728	−1.2773	19.06
5	(Positive)	0.9179	1.0457	1.0451	1.0708	7.08
	(Negative)	−1.2358	−1.5034	−0.9291	−0.9879	6.33

of the model considered here. This makes $F_{ENV} = 1.14$. This factor is multiplied by the Cp_e and is presented in Table 5.

The approach described by Gierson et al. (2015) was followed to compute the gust factors (i.e., G) through area averaging and peak estimation. The experimental Cp values used in this study comparison are the envelope of 3s Cp values obtained after the application of the PTS method. These Cp values at each tap location are area-averaged over the entire area of each zone and presented in Table 5.

As detailed in Table 5, ASCE 7-16 underestimates the positive Cp values on Models A and B at Zones 4 and 5, while the Eurocode estimates Model A correctly but underestimates Model B. The ASCE 7-16 gives conservative negative Cp for Models A and B at Zone 5 but underestimates them at Zone 4. The Eurocode overestimates the negative Cp values in Zones 4 and 5 of Models A and B. It also indicates that the Cp values on Model B are higher than those on Model A at the two zones considered.

Accelerations

To understand the dynamics of the curtain wall system, accelerometers were installed on the external glass in locations, as shown in Fig. 11. This study adopted the eigenvalue realization algorithm-observer Kalman filter identification for output-only systems (ERA-OKID-OO) developed by Chang and Pakzad (2014). The analysis indicated that the 4.2 Hz natural frequency corresponds to the global response of the entire structure including the supporting steel structure and the curtain wall, while the higher 17-Hz frequency corresponds to the local response of the curtain wall. This was also confirmed by a detailed finite-element modeling of the curtain wall unit.

However, the results presented in this paper are from the entire time history of the acceleration response without filtering out the 4.2 Hz. All the accelerometer time histories were stationary and hence rms were calculated for each wind direction. For this paper, Accelerometer 3 is considered as it is in the middle of a typical (center) panel. Fig. 17(a) shows the acceleration rms in the Z (out-of-plane) direction for various wind speeds obtained for 0° wind direction. Fig. 17(b) shows the rms for various wind directions obtained for 31.30 m/s of wind speed at the roof height. The data is then converted into frequency domain to identify the natural frequency of the tested curtain wall sample (the first mode of vibration frequency is obtained where the first spike in the power spectral density is observed). Overall, Model B's power content is higher compared with Model A. Fig. 17(c) shows a clear spike near 4.2 and 17 Hz for Models A and B.

These results signify the importance of studying dynamic effects in systems such as curtain walls. As explained previously, the 1-Hz criteria of ASCE 7-16 again could not be used for curtain wall design for vibration against wind. From a design perspective, the dynamic amplification factor (DAF) values were calculated by splitting the time history into quasi-steady background response and resonant response using the formula

$$\mathrm{DAF} = \frac{\hat{R}}{\bar{R} + R'_B} \tag{6}$$

where $\hat{R}$ = peak response (acceleration or strain); $\bar{R}$ = mean response; and R'_B= background response.

To compute the DAF values, the authors used the methodology laid out in Elawady et al. (2017). The DAF values are provided in Fig. 17(d) for wind speeds at 0° wind direction and Fig. 17(e) for wind directions at 22.35 m/s wind speed.

In summary, Model B showed higher rms and DAF in comparison with Model A for the tests. The common spikes near 4.2 and 17 Hz in PSD show that the natural frequency of the system is not affected by the addition of vertical protrusions. Although the vertical protrusions reduce wind fluctuations as shown by the Cp rms plots in Fig. 16, they increase the stiffness of the frame holding the glass thereby increasing the dynamic response of the glass which is also apparent in DAF values shown in Fig. 17(d). Nakagami (2003) similarly observed a dependence of the motion of glass to the stiffness of its supporting system.

Strains

In addition to the effects on wind pressure distributions on walls, vertical protrusions can influence the general structural stiffness of curtain wall units. Fig. 18 shows the strain values at strain gauge 5 (S5) and strain gauge 2 (S2) on the mullion [see Fig. 11(a) for the location of strain gauges] at 40.2 m/s wind speed. The positive strains indicate tension and negative strains indicate compression. Figs. 18(a and b) show the variation of mean strains with wind direction. The maximum strains are observed at 0° for S5, while maximum strains are observed at 315° for S2 due to their position relative to the wind direction. The strain results also indicate that the vertical protrusions increase the joint stiffness between panels: a smaller strain was recorded in Model B at S5 [J2 in Fig. 5(b)] as observed in Fig. 18(a) where there is a higher difference between the strains on Models A and B.

At the mullion joints with no vertical protrusions [e.g., J1 and J5 in Fig. 5(b)], the Model B configuration shows higher strains as expected due to the increased pressures as observed for S2 except at 0° wind direction where the vertical protrusions do not have a lot of impact on the flow. The difference in strain direction in S2 for 45° wind direction is due to flow separation occurring because of the fins. No dynamic amplifications were observed in the mullions of the two model configurations tested. An increase in strains with increasing wind speeds was observed as shown in Fig. 18(c), indicating higher wind loads.

WDR Performance of Single-Skin Façades

The WDR water intrusion test is to evaluate the effect of combined realistic rain and WIV on the water intrusion of the façade unit. Only three wind directions were considered and reported in this study, as all aforementioned water penetration testing provisions recommend the 0° wetting direction. Testing Model A for wind-driven rain intrusion was conducted as a baseline study. While no rain measurements were taken for Model B, it was envisioned that Model B will have more water intrusion due to the higher vibrations observed in the testing.

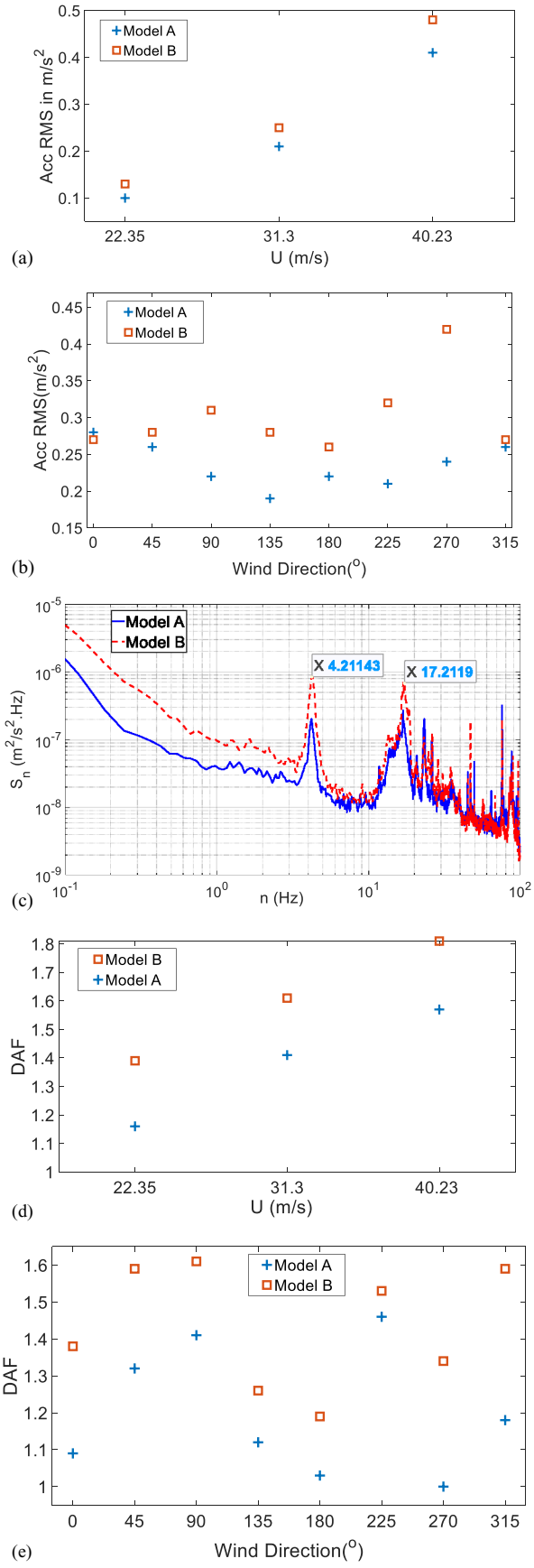

Fig. 17. Acceleration analysis: (a) A3-Z rms versus wind speed; (b) A3-Z rms versus wind direction; (c) PSD showing a 4.2-Hz spike; (d) A3-Z DAF versus wind speed; and (e) A3-Z DAF versus wind direction.

Joints 2, 3, and 4 [J2, J3, and J4 shown in Fig. 5(b)], and windowsill were identified as the critical locations of possible water intrusion. The volume of water intrusion at each joint is presented in Fig. 19. At the 22.3 and 31.3 m/s wind speeds, water intrusion was under 5 mL (based on weight change of the absorbent pads) at all the three joints for the tested wind directions. Also, no water intrusion was visible. At 40.2 m/s, water intrusion was observed at Joint 3 and the windowsill, with the highest water intrusion occurring at 0°. The results suggest that Joint 3 is the most vulnerable joint where the operable part is located, while the area around the window is very vulnerable to water intrusion, as evidenced by the larger quantity of water intrusion through the windowsill. High water intrusion at window frames was also observed by Vutukuru et al. (2020).

Correlation of WDR and WIV

Fig. 20(a) shows the total water intrusion per minute, for all three wind directions recorded and the three wind speeds, while Fig. 20(b) shows the water intrusion per minute for each wind direction. The test results indicate an increase in the water intrusion with wind speed. A similar observation was also made for the curtain wall measured vibrations. This indicates a positive correlation between WIV and WDR performance of the curtain wall system. In addition, careful attention should be paid when adding shading devices that may alter the behavior and response of curtain wall systems.

Concluding Remarks and Recommendation for Further Studies

Concluding Remarks

The current study investigated the influence of vertical protrusions on the performance of a single-skin curtain wall system, as well as the combined impact of WIV and WDR on the water intrusion into the façade system. The following can be concluded from this study for the curtain wall system used:

1. Vertical protrusions influence the Cp_{peak} values and pattern on claddings as they increase the overall positive Cp_{peak} (by as much as 7.24%) and increase (in magnitude) negative Cp_{peak} (by as much as 19.06%) on the curtain wall. They also reduce suction in wind directions parallel to the curtain wall surface.
2. The vertical protrusions increase the positive envelope Cp (by as much as 30%) and negative envelope Cp (by as much as 26%) at regions adjacent to the protrusion. However, they reduce wind fluctuations behind the protrusion at oblique wind directions.
3. Vertical protrusions contribute to the increase of stiffness at the joints. This leads to higher vibrations of the glazing in curtain walls, as evident in the higher accelerations and higher acceleration dynamic amplification factors observed in the glazing of Model B.
4. Acceleration dynamic amplification factors increase with wind speed and are usually higher on the model with vertical protrusion at all wind directions. Oblique wind directions give the highest resonant response for the glazing on Model B. At the highest wind speed tested, the resonant response on the glazing is in the order of 58% and 80% for Model A and Model B, respectively.
5. Water intrusion was observed at all wind speeds higher than about 20 m/s. However, more water intrusion was observed in the window region. This suggests that areas with openings on

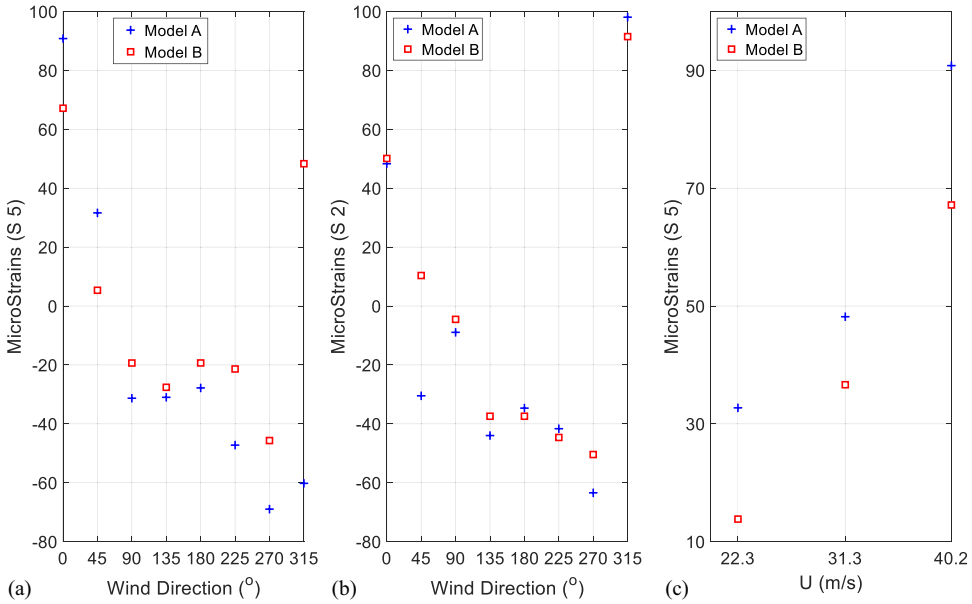

Fig. 18. Mean strains plots: (a) wind direction versus S5 strains; (b) wind direction versus S2 strains; and (c) wind speed versus S5 strains (at 0° wind direction).

the curtain wall such as the operable parts are more vulnerable to water intrusion, especially at high wind speeds.

6. Higher wind speeds lead to higher vibrations that result in more water intrusion. The acceleration rms and rate of water penetration both indicate an increase with wind speed. The sharp rise in water penetration rate from 31.3 to 40.2 m/s was due to an increase in water penetration through the operable window.

The findings of this study indicate that vertical protrusions have an influence on the curtain wall system performance. The study suggests that manufacturers and standard-setting agencies should consider the following: (1) joints around the protrusions might require more attention and seal based on the higher pressure coefficients observed around the vertical protrusions in this study; (2) glass in curtain walls with vertical protrusions should be designed with an expectation of higher vibrations; (3) joints around windows require attention, especially for units designed for high-wind velocity zones as they are vulnerable at high wind speeds to water intrusion.

Recommendation for Further Study

Specifically, for the model setup in this study, the 4.2 Hz natural frequency corresponds to the entire structure, while the 17 Hz was attributed to the curtain wall. This implies the first eigenmode will be determined by where and how the curtain wall is attached, and the dynamic response of the curtain wall will be greatly influenced by the building/supporting structure. Further investigation into how the support structure affects the dynamic behavior of the curtain wall is recommended for future studies. To further

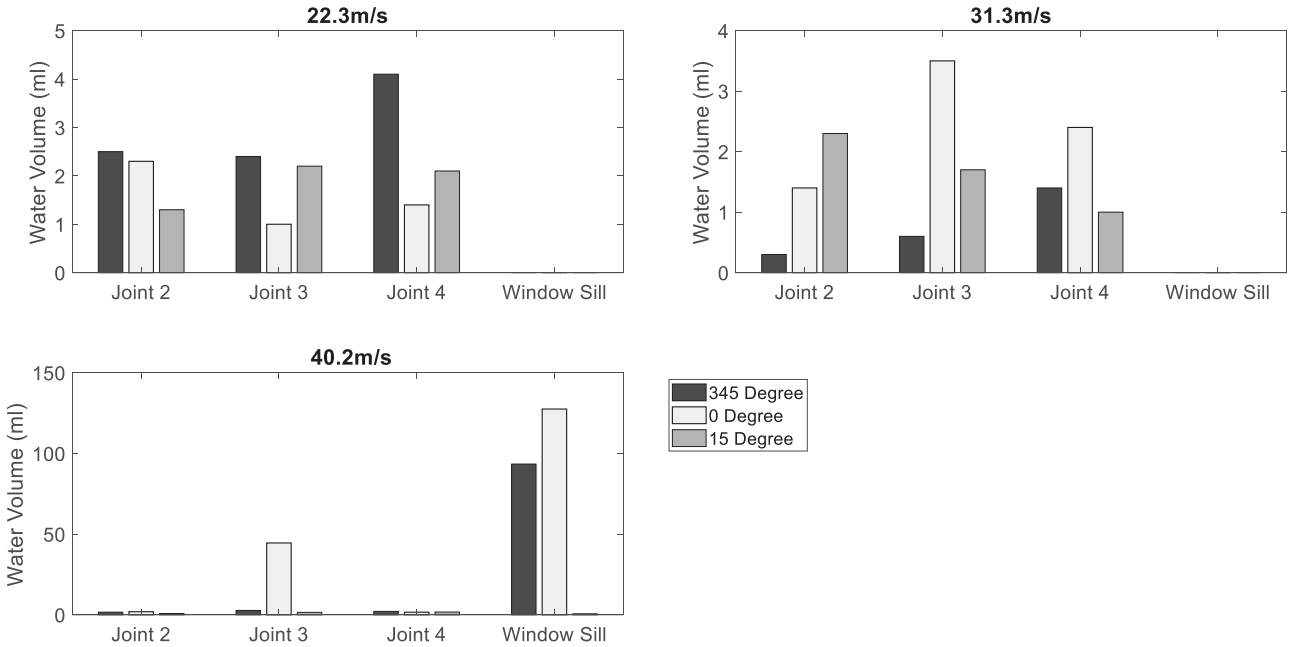

Fig. 19. Water intrusion at joints and windowsill tested for three different wind directions.

J. Archit. Eng., 2023, 29(2): 04023003

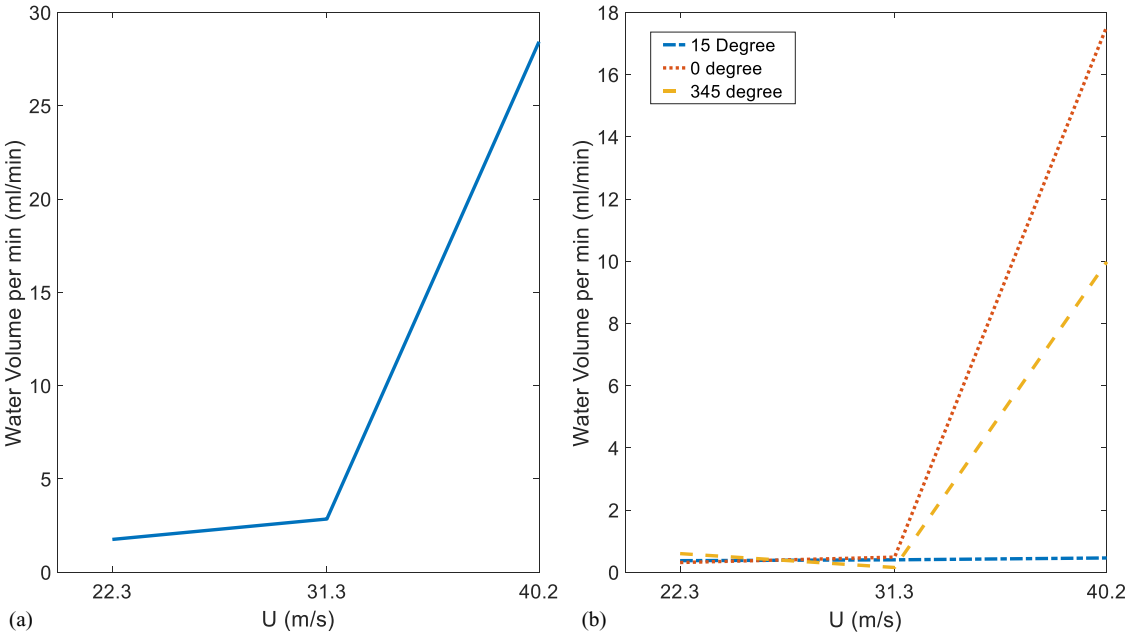

Fig. 20. Water intrusion per minute at wind speeds of 22.3, 31.3 and 40.2 m/s for Model A: (a) total water penetration; and (b) water penetration per wind direction.

ascertain the effect of depth and shape of vertical protrusions on the wind pressure and water intrusion in cladding systems, other configurations of vertical protrusions should be tested. In addition, the effect of supporting structures on the response of the curtain wall must be further investigated. Further studies to investigate the sufficiency of uniform wind profiles with grid-generated turbulence in testing curtain walls is also recommended, as this might provide a better test bed for curtainwall quality tests that replicate the ABL, which can be adopted by manufacturers.

Data Availability Statement

Some or all data that support the findings of this study are available from the corresponding author upon reasonable request.

Acknowledgments

These tests were conducted at the NHERI Wall of Wind Experimental Facility (National Science Foundation Award No. 1520853 and No. 2037899). This paper is based upon work sponsored by the US National Science Foundation under the awards NSF IIP1841503,1841523 and I/UCRC Wind Hazard and Infrastructure Performance #2019-04. The authors also would like to thank Permasteelisa group for providing the curtain wall and curtain wall fixers. The authors also appreciate Roy-Liu Marques, James Erwin, and Walter Conklin for their support in instrumenting the model specimen. The opinions, findings, conclusions, or recommendations expressed in this article are solely those of the authors and do not represent the opinions of the funding agencies.

References

AAMA (American Architectural Manufacturers Association). 2005. *Standard test method for water intrusion of windows, curtain walls and doors using dynamic pressure*. AAMA 501.1-05. Schaumburg, IL: AAMA.

ASCE. 2016. *Minimum design loads for buildings and other structures*. ASCE 7-16. Reston, VA: ASCE.

ASTM. 2009. *Standard test method for field determination of water intrusion of exterior windows, skylights, doors, and curtain walls by uniform or cyclic static Air pressure difference*, 1–5. ASTM E1105-15, 00(Reapproved). West Conshohocken, PA: ASTM.

ASTM. 2016a. *Standard test method for water intrusion of exterior windows, skylights, doors, and curtain walls by uniform static air pressure difference*, 1–5. ASTM E331-00, 00(Reapproved). West Conshohocken, PA: ASTM.

ASTM. 2016b. *Standard test method for water intrusion of exterior windows, skylights, doors, and curtain walls by uniform static air pressure*. ASTM E547-00. West Conshohocken, PA: ASTM.

Azzi, Z., F. Habte, K. S. Vutukuru, A. G. Chowdhury, and M. Moravej. 2020. "Effects of roof geometric details on aerodynamic performance of standing seam metal roofs." *Eng. Struct.* 225: 111303. https://doi.org/10.1016/j.engstruct.2020.111303.

Baheru, T., A. Gan Chowdhury, G. Bitsuamlak, F. J. Masters, and A. Tokay. 2014. "Simulation of wind-driven rain associated with tropical storms and hurricanes using the 12-fan wall of wind." *Build. Environ.* 76: 18–29. https://doi.org/10.1016/j.buildenv.2014.03.002.

Baskaran, B. A., and W. C. Brown. 1995. "Dynamic evaluation of the building envelope for wind and wind-driven rain performance." *J. Therm. Insul. Build. Envelopes* 18: 261–275. https://journals.sagepub.com/doi/pdf/10.1177/109719639501800306.

Blocken, B., and J. Carmeliet. 2004. "A review of wind-driven rain research in building science." *J. Wind Eng. Ind. Aerodyn.* 92 (13): 1079–1130. https://doi.org/10.1016/j.jweia.2004.06.003.

Cain, J. H., D. Banks, and C. P. Petersen. 2015. "Wind Loads on Utility Scale Solar PV Power Plants." In *Proc., of SEAOC Convention*. Sacramento, CA: Structural Engineers Association of California.

CEN (European Committee for Standardization). 2000. *Curtain walling - Watertightness - Laboratory test under static pressure*. EN 12155:2000. Brussels, Belgium: CEN.

CEN (European Committee for Standardization). 2001a. *Hygrothermal performance of building components and building elements — determination of the resistance of external wall systems to driving rain under pulsating air pressure*. EN 12865. Brussels, Belgium: CEN.

CEN (European Committee for Standardization). 2001b. *Curtain walling — Watertightness — Site test*. EN 13051. Brussels, Belgium: CEN.

CEN (European Committee for Standardization). 2011a. *Actions on structures part 1–4: General actions — Wind actions*. Eurocode 1, EN 1991-1-4:2005+A1:2010. Brussels, Belgium: CEN.

CEN (European Committee for Standardization). 2011b. *Curtain walling — Watertightness — Laboratory test under dynamic condition of air pressure and water spray*. EN 13050:2011. Brussels, Belgium: CEN.

Chand, I., and P. K. Bhargava. 1997. "Laboratory studies on the effect of external protrusions on wind pressure distribution on low-rise buildings." *Archit. Sci. Rev.* 40 (4): 133–137. https://doi.org/10.1080/00038628.1997.9696823.

Chang, M., and S. Pakzad. 2014. "Observer Kalman filter identification for output-only systems using interactive structural modal identification toolsuite." *J. Bridge Eng.* 19 (5): 04014002. https://doi.org/10.1061/(ASCE)BE.1943-5592.0000530.

Cho, J., C. Yoo, and Y. Kim. 2014. "Viability of exterior shading devices for high-rise residential buildings: Case study for cooling energy saving and economic feasibility analysis." *Energy Build.* 82: 771–785. https://doi.org/10.1016/j.enbuild.2014.07.092.

Choi, E. C. C. 1993. "Simulation of wind-driven-rain around a building." In *Proc., 1st Int. Symp. on Computational Wind Engineering*, edited by S. Murakami, 721–729. Amsterdam, The Netherlands: Elsevier.

Choi, E. C. C. 2008. "The effect of wind-driven rain on cladding pressure of buildings under wind and rain conditions." In *Proc., BBAA VI Int. Colloquium on Bluff Bodies Aerodynamics and Applications*, 1–4. Milano, Italy: BBAA. http://bbaa6.mecc.polimi.it/uploads/abstract_files/NB05_STAMPA5.pdf.

Chowdhury, A. G., K. S. Vutukuru, and M. Moravej. 2018. "Full- and large-scale experimentation using the wall of wind to mitigate wind loading and rain impacts on buildings and infrastructure systems." In *Proc., 11th Structural Engineering Convention*. *New Delhi, India*: Indian Association for Structural Engineering. http://www.iastructe.co.in/.

Chowdhury, A. G., I. Zisis, P. Irwin, G. Bitsuamlak, J. P. Pinelli, B. Hajra, and M. Moravej. 2017. "Large-scale experimentation using the 12-fan wall of wind to assess and mitigate hurricane wind and rain impacts on buildings and infrastructure systems." *J. Struct. Eng.* 143 (7): 04017053. https://doi.org/10.1061/(ASCE)ST.1943-541X.0001785.

Cornick, S. M., and M. A. Lacasse. 2005. "A review of climate loads relevant to assessing the watertightness performance of walls, windows, and wall-window interfaces." *J. ASTM Int.* 2 (10): 1–16. https://doi.org/10.1520/JAI12505.

Derome, D., A. Kubilay, T. Defraeye, B. Blocken, and J. Carmeliet. 2017. "Ten questions concerning modeling of wind-driven rain in the built environment." *Build. Environ.* 114: 495–506. https://doi.org/10.1016/J.BUILDENV.2016.12.026.

Durst, C. S. 1960. "Wind speeds over short periods of time." *Meteorol. Mag.* 89: 181–187.

Elawady, A., H. Aboshosha, A. El Damatty, G. Bitsuamlak, and H. Hangan. 2017. "Aero-elastic testing of multi-spanned transmission line subjected to downbursts." *J. Wind Eng. Ind. Aerodyn.* 169: 194–216. https://doi.org/10.1016/j.jweia.2017.07.010.

ESDU (Engineering Sciences Data Unit). 2001. *Characteristics of the atmospheric boundary layer, Part II: Single point data for strong winds (neutral atmosphere)*, ESDU Item 85020. London: ESDU.

Estephan, A., A. G. Chowdhury, and P. Irwin. 2021. "A new experimental-numerical approach to estimate peak wind loads on roof-mounted photovoltaic systems by incorporating inflow turbulence and dynamic effects." *Eng. Struct.* 252: 113739. https://doi.org/10.1016/j.engstruct.2021.113739.

Evangelisti, L., C. Guattari, F. Asdrubali, and R. de Lieto Vollaro. 2020. "An experimental investigation of the thermal performance of a building solar shading device." *J. Build. Eng.* 28: 101089. https://doi.org/10.1016/j.jobe.2019.101089.

FEMA. 2005. Vol. 488 of *Hurricane Charley in Florida: observations, recommendations, and technical guidance*, 1–24. Washington, DC: FEMA.

FEMA. 2006. *Hurricane Katrina in the Gulf Coast (FEMA 549)*, Washington, DC: Federal Emergency Management Agency (FEMA).

Fronstin, P., and A. G. Holtmann. 1994. "The determinants of residential property damage caused by Hurricane Andrew." *J. South. Econ.*, 61 (2): 387–397. https://doi.org/10.2307/1059986.

Gierson, M. L., B. M. Phillips, and D. Duthinh. 2015. "Evaluation of ASCE 7-10 wind velocity pressure coefficients on the components and cladding of low-rise buildings using recent wind tunnel testing data." In *Proc., 6th Int. Conf. on Advances in Experimental Structural Engineering, 11th Int. Workshop on Advanced Smart Materials and Smart Structural Technology*. Urbana, IL: University of Illinois, Urbana-Champaign. http://sstl.cee.illinois.edu/papers/aeseancrisst15/189_Gierson_Evaluation.pdf.

Guha, T. K., R. N. Sharma, and P. J. Richards. 2011. "Internal pressure dynamics of a leaky building with a dominant opening." *J. Wind Eng. Ind. Aerodyn.* 99: 1151–1161. https://doi.org/http://doi.org/10.1016/j.jweia.2011.09.002.

Habte, F., M. Asghari Mooneghi, A. Gan Chowdhury, and P. Irwin. 2015. "Full-scale testing to evaluate the performance of standing seam metal roofs under simulated wind loading." *Eng. Struct.* 105: 231–248. https://doi.org/10.1016/j.engstruct.2015.10.006.

ICC (International Code Council). 2017a. *Testing application standard (TAS) 202-94 criteria for testing impact and nonimpact resistant building envelope components using uniform static air pressure*. 2017 Florida Building Code—Test Protocols for High Velocity Hurricane Zone, 978-1-60983-688-7. Wasington, DC: ICC.

ICC (International Code Council). 2017b. *Testing application standard (TAS) 203-94 criteria for testing products subject to cyclic wind pressure loading.* 2017 Florida Building Code—Test Protocols for High Velocity Hurricane Zone, 978-1-60983-688-7. Washington, DC: ICC.

Irwin, H. P. A. H., K. R. Cooper, and R. Girard. 1979. "Correction of distortion effects caused by tubing systems in measurements of fluctuating pressures." *J. Wind Eng. Ind. Aerodyn.* 5 (1): 93–107. https://doi.org/https://doi.org/10.1016/0167-6105(79)90026-6.

Kubilay, A., D. Derome, B. Blocken, and J. Carmeliet. 2015. "Wind-driven rain on two parallel wide buildings: Field measurements and CFD simulations." *J. Wind Eng. Ind. Aerodyn.* 146: 11–28. https://doi.org/10.1016/j.jweia.2015.07.006.

Liu, J., Y. Hui, Q. Yang, and Y. Tamura. 2020. "Flow field investigation for aerodynamic effects of surface mounted ribs on square-sectioned high-rise buildings." *J. Wind Eng. Ind. Aerodyn.* 211: 104551. https://doi.org/10.1016/j.jweia.2021.104551.

Liu, M., Q. Sheng, and S. Hong. 2019. "Large eddy simulation of wind-driven rain effects on a large span retractable roof stadium." *J. Wind Eng. Ind. Aerodyn.* 195: 104009. https://doi.org/10.1016/j.jweia.2019.104009.

Mandalaki, M., K. Zervas, T. Tsoutsos, and A. Vazakas. 2012. "Assessment of fixed shading devices with integrated PV for efficient energy use." *Sol Energy* 86 (9): 2561–2575. https://doi.org/http://dx.doi.org/10.1016/j.solener.2012.05.026.

Maruta, E., M. Kanda, and J. Sato. 1998. "Effects on surface roughness for wind pressure on glass and cladding of buildings." *J. Wind Eng. Ind. Aerodyn.* 74–76: 651–663. https://doi.org/10.1016/S0167-6105(98)00059-2.

Mooneghi, A. M., P. Irwin, and A. Gan Chowdhury. 2016. "Partial turbulence simulation method for predicting peak wind loads on small structures and building appurtenances." *J. Wind Eng. Ind. Aerodyn.* 157: 47–62. https://doi.org/10.1016/j.jweia.2016.08.003.

Moravej, M. 2018. "Investigating scale effects on analytical methods of predicting peak wind loads on buildings." Ph.D. thesis, Dept. of Civil and Environmental Engineering, Florida International Univ. https://digitalcommons.fiu.edu/etd/3799.

Moravej, M., A. G. Chowdhury, P. Irwin, I. Zisis, and G. Bitsuamlak. 2015. "Dynamic effects of wind loading on photovoltaic systems." In *Proc., of 14th Int. Conf. on Wind Engineering*. Tokyo, Japan: International Association for Wind Engineering. https://www.icwe14.org/.

Naeiji, A. 2017. "Wind loads on residential rooftop solar photovoltaic panels." Ph.D. thesis, Dept. of Civil and Environmental Engineering, Florida International Univ.

Nakagami, Y. 2003. "Probabilistic dynamics of wind excitation on glass façade." Ph.D. thesis, Dept. of Civil Engineering and Geodesy, Technische Universität Darmstadt. http://elib.tu-darmstadt.de/diss/000343.

NOAA National Centers for Environmental Information (NCEI). 2019. "Billion-dollar weather and climate disasters." Accessed July 12, 2019. https://www.ncdc.noaa.gov/billions/events/US/1980-2019.

Orr, S. A., and H. Viles. 2018. "Characterisation of building exposure to wind-driven rain in the UK and evaluation of current standards." *J. Wind Eng. Ind. Aerodyn.* 180: 88–97. https://doi.org/10.1016/J.JWEIA.2018.07.013.

Pariafsai, F. 2016. "A review of design considerations in glass buildings." *Front. Archit. Res.* 5 (2): 171–193. https://doi.org/10.1016/j.foar.2016.01.006.

Pérez-Bella, J. M., J. Domínguez-Hernández, B. Rodríguez-Soria, J. J. del Coz-Díaz, E. Cano-Suñén, and A. Navarro-Manso. 2013. "An extended method for comparing watertightness tests for facades." *Build. Res. Inf.* 41 (6): 706–721. https://doi.org/10.1080/09613218.2013.823538.

Rofail, A. W., and K. C. S. Kwok. 1999. "The effect of sunshading elements on cladding pressures." In *Proc., 10th Int. Conf. on Wind Engineering. Tokyo, Japan*: International Association for Wind Engineering.

Sayed, M. A. A. E. D. A., and M. A. Fikry. 2019. "Impact of glass facades on internal environment of buildings in hot arid zone." *Alexandria Eng. J.* 58 (3): 1063–1075. https://doi.org/10.1016/j.aej.2019.09.009.

Stathopoulos, T., and X. Zhu. 1990. "Wind pressures on buildings with mullions." *J. Struct. Eng.* 116 (8): 2272–2291. https://doi.org/10.1061/(asce)0733-9445(1990)116:8(2272).

Strobel, K., and D. Banks. 2014. "Effects of vortex shedding in arrays of long inclined flat plates and ramifications for ground-mounted photovoltaic arrays." *J. Wind Eng. Ind. Aerodyn.* 133: 146–149. https://doi.org/10.1016/j.jweia.2014.06.013.

St. Pierre, L. M., G. A. Kopp, D. Surry, and T. C. E. Ho. 2005. "The UWO contribution to the NIST aerodynamic database for wind loads on low buildings: Part 2. Comparison of data with wind load provisions." *J. Wind Eng. Ind. Aerodyn.* 93 (1): 31–59. https://doi.org/10.1016/j.jweia.2004.07.007.

Taniike, Y. 1992. "Interference mechanism for enhanced wind forces on neighboring tall buildings." *J. Wind Eng. Ind. Aerodyn.* 43 (1-3): 1073–1083. https://doi.org/10.1016/0167-6105(92)90114-P.

Tokay, A., P. G. Bashor, E. Habib, and T. Kasparis. 2008. "Raindrop size distribution measurements in tropical cyclones." *Mon. Weather Rev.* 136 (5): 1669–1685. https://doi.org/10.1175/2007MWR2122.1.

Tokay, A., W. A. Petersen, P. Gatlin, and M. Wingo. 2013. "Comparison of raindrop size distribution measurements by collocated disdrometers." *J. Atmos. Ocean* 30 (8): 1672–1690. https://doi.org/10.1175/JTECH-D-12-00163.1.

Van Den Bossche, N., M. A. Lacasse, and A. Janssens. 2013a. "A uniform methodology to establish test parameters for watertightness testing. Part I: A critical review." *Build Environ.* 63: 145–156. https://doi.org/10.1016/j.buildenv.2012.12.003.

Van Den Bossche, N., M. A. Lacasse, and A. Janssens. 2013b. "A uniform methodology to establish test parameters for watertightness testing part II: Pareto front analysis on co-occurring rain and wind." *Build Environ.* 63: 157–167. https://doi.org/10.1016/j.buildenv.2012.12.019.

Vutukuru, K. S., K. J. Alawode, A. Bakhtiari, A. Elawady, S. J. Lee, A. G. Chowdhury, and G. Lori. 2021. "Full-scale experimental testing to investigate wind-induced vibrations on curtain wall systems." In *Proc., 11th Int. Structural Engineering and Convention*, edited by S. El Baradei, A. Abodonya, A. Singh, and S. Yazdani. Fargo, ND: ISEC Press.

Vutukuru, K. S., M. Moravej, A. Elawady, and A. G. Chowdhury. 2020. "Holistic testing to determine quantitative wind-driven rain intrusion for shuttered and impact resistant window." *J. Wind Eng. Ind. Aerodyn.* 206: 104359. https://doi.org/10.1016/j.jweia.2020.104359.

Yang, Q., Z. Liu, Y. Hui, and Z. Li. 2020. "Modification of aerodynamic force characteristics on high-rise buildings with arrangement of vertical plates." *J. Wind Eng. Ind. Aerodyn.* 200: 104155. https://doi.org/10.1016/j.jweia.2020.104155.

Yu, Y., T. Liu, Q. Zhang, and B. Yang. 2017. "Wind-induced response of an L-shaped cable support glass curtain wall." *Shock Vib.* 2017: 4163045. https://doi.org/10.1155/2017/4163045.

Yuan, K., Y. Hui, and Z. Chen. 2018. "Effects of facade appurtenances on the local pressure of high-rise building." *J. Wind Eng. Ind. Aerodyn.* 178: 26–37. https://doi.org/10.1016/j.jweia.2018.05.004.

Zheng, J., Q. Tao, and L. Li. 2020. "Wind pressure coefficient on a multistorey building with external shading louvers." *Appl. Sci.* 10 (3): 1128. https://doi.org/10.3390/app10031128.

Zhengnong, L., L. Diefeng, S. Wenhai, L. Zhiqi, and L. Xiaohan. 2011. "Field measurement of wind-induced stress on glass facade of a coastal high-rise building." *Sci. China Technol. Sci.* 54 (10): 2587–2596. https://doi.org/10.1007/s11431-011-4512-z.